CHAPTER 10

MESHFREE METHODS IN COMPUTATIONAL STOCHASTIC MECHANICS

SHARIF RAHMAN

Department of Mechanical and Industrial Engineering
The University of Iowa, Iowa City, IA 52245, USA
E-mail: rahman@engineering.uiowa.edu

This chapter provides an exposition of stochastic meshfree methods that involves deterministic meshfree formulation, spectral representation of random fields, multivariate function decomposition, statistical moment analysis, and reliability analysis. Numerical results indicate that stochastic meshfree methods, employed in conjunction with dimension-reduction and decomposition methods, yield accurate and computationally efficient estimates of statistical moments and reliability. Although significant strides have been made, breakthrough research on enhancing speed and robustness of meshfree methods is essential for their successful implementation into stochastic mechanics.

1. Introduction

During the last decade, much attention has been focused on collocation[1,2]- or Galerkin-based[3–8] meshfree or meshless methods to solve computational mechanics problems without using a structured grid. Among these methods, the element-free Galerkin method (EFGM)[4] is particularly appealing, due to its simplicity and use of a formulation that corresponds to the well-established finite element method (FEM). Similar to other meshfree methods, EFGM employs moving least-squares approximation[9] that permits the resultant shape functions to be constructed entirely in terms of arbitrarily placed nodes. Since no element connectivity data are needed, burdensome meshing or remeshing required by FEM is avoided. This issue is particularly important for crack propagation in solids for which FEM may be ineffective in addressing substantial remeshing.[10–15] Hence, EFGM and other meshfree methods provide an attractive alternative to FEM in solving computational-mechanics problems.

However, most meshfree development has focused on deterministic problems. Research in probabilistic modeling using EFGM or other meshfree methods has not been widespread and is only now gaining attention.[16–20] For example, using the perturbation and first-order reliability methods, Rahman and Rao[16,17] developed stochastic meshless formulations to predict both the second-moment and reliability of stochastic structures. An alternative approach involving spectral representation of random fields and Neumann series expansion has also appeared for second-moment meshless analysis.[18] Due to their inherent advantages,

most stochastic meshless development has been focused on linear-elastic[19,20] and nonlinear[21] fracture-mechanics problems. More recently, new stochastic solutions integrating meshfree formulation and dimension-reduction techniques and decomposition methods have been reported.[22–24] Nevertheless, meshfree methods for probabilistic analysis present a rich and relatively unexplored area for future research in computational stochastic mechanics.

This chapter provides an exposition of meshfree methods for stochastic mechanics and reliability applications. Section 2 reviews deterministic formulation of EFGM. Section 3 discusses the Karhunen-Loève representation of a random field, meshfree solution of an integral equation, and modeling of Gaussian and translation fields. Section 4 informs the reader on function decomposition that facilitates lower-variate approximations of a general multivariate function. Using function decomposition, dimension-reduction methods for statistical moment analysis are presented in Sec. 5. A Monte Carlo simulation using response surface models of lower-variate approximations is examined in Sec. 6. Several numerical examples are presented to illustrate various methods developed. Finally, Sec. 7 concludes the chapter with the impact of current research and future research needs in stochastic meshfree analysis.

2. The Element-Free Galerkin Method

2.1. *Moving least squares and meshless shape function*

Consider a real-valued, continuous, differentiable function $u(\boldsymbol{x})$ over a domain $\mathcal{D} \subset \mathbb{R}^K$, where $K = 1, 2$, or 3. Let $\mathcal{D}_x \subseteq \mathcal{D}$ denote a subdomain describing the neighborhood of a point $\boldsymbol{x} \in \mathcal{D} \subset \mathbb{R}^K$. A moving least-squares (MLS) approximation $u^h(\boldsymbol{x})$ of $u(\boldsymbol{x})$ is[9]

$$u^h(\boldsymbol{x}) = \sum_{i=1}^{m} p_i(\boldsymbol{x}) a_i(\boldsymbol{x}) = \boldsymbol{p}^T(\boldsymbol{x})\boldsymbol{a}(\boldsymbol{x}), \tag{1}$$

where $\boldsymbol{p}^T(\boldsymbol{x}) = \big\{p_1(\boldsymbol{x}), \ldots, p_m(\boldsymbol{x})\big\}$ is a vector of complete basis functions of length m and $\boldsymbol{a}(\boldsymbol{x}) = \big\{a_1(\boldsymbol{x}), \ldots, a_m(\boldsymbol{x})\big\}^T$ is a vector of unknown parameters that depend on $\boldsymbol{x}$. For example, basis functions commonly used in two-dimensional ($K = 2$) solid mechanics with $x_1 - x_2$ coordinates are $\boldsymbol{p}^T(\boldsymbol{x}) = \big\{1, x_1, x_2\big\}$; $m = 3$ and $\boldsymbol{p}^T(\boldsymbol{x}) = \big\{1, x_1, x_2, x_1^2, x_1x_2, x_2^2\big\}$; $m = 6$, which represent linear and quadratic basis functions, respectively. The basis functions need not be polynomial. When solving problems involving cracks, trigonometric basis functions consistent with singular crack-tip fields have been developed for both linear-elastic[11] and nonlinear[14] fracture-mechanics applications.

The coefficient vector $\boldsymbol{a}(\boldsymbol{x})$ in Eq. (1) is determined by minimizing a weighted error norm, defined as:

$$J(\boldsymbol{x}) \equiv \sum_{I=1}^{l} w_I(\boldsymbol{x})\big[\boldsymbol{p}^T(\boldsymbol{x}_I)\boldsymbol{a}(\boldsymbol{x}) - d_I\big]^2 = [\boldsymbol{P}\boldsymbol{a}(\boldsymbol{x}) - \boldsymbol{d}]^T\boldsymbol{W}[\boldsymbol{P}\boldsymbol{a}(\boldsymbol{x}) - \boldsymbol{d}], \tag{2}$$

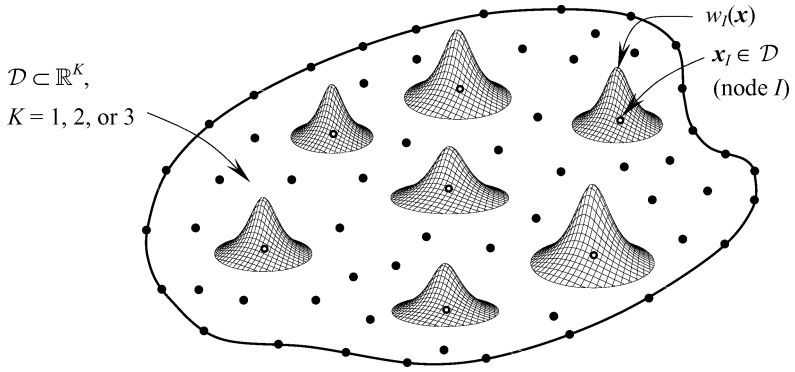

Fig. 1. A schematic illustration of meshfree discretization and weight functions with compact support.

where $\boldsymbol{x}_I$ denotes the coordinates of node I, $\boldsymbol{d}^T = \{d_1, \ldots, d_l\}$ with d_I representing the nodal parameter for node I, $\boldsymbol{W} = \text{diag}[w_1(\boldsymbol{x}), \ldots, w_l(\boldsymbol{x})]$ with $w_I(\boldsymbol{x})$ being the weight function associated with node I, such that $w_I(\boldsymbol{x}) > 0$ for all $\boldsymbol{x}$ in the support $\mathcal{D}_{\boldsymbol{x}}$ of $w_I(\boldsymbol{x})$ and *zero* otherwise, l is the number of nodes in $\mathcal{D}_{\boldsymbol{x}}$ for which $w_I(\boldsymbol{x}) > 0$, and $\boldsymbol{P} = [\boldsymbol{p}^T(\boldsymbol{x}_1), \ldots, \boldsymbol{p}^T(\boldsymbol{x}_l)] \in \mathbb{L}(\mathbb{R}^l \times \mathbb{R}^m)$. The weight function has a compact support and is schematically depicted in Fig. 1. A number of weight functions are available in the current literature.[3–21] For example, a weight function proposed by Rao and Rahman is[12]

$$w_I(\boldsymbol{x}) = \begin{cases} \dfrac{\left(1+\beta^2 \frac{z_I^2}{z_{mI}^2}\right)^{-\left(\frac{1+\beta}{2}\right)} - \left(1+\beta^2\right)^{-\left(\frac{1+\beta}{2}\right)}}{1-\left(1+\beta^2\right)^{-\left(\frac{1+\beta}{2}\right)}}, & z_I \le z_{mI} \\ 0, & z_I > z_{mI} \end{cases}, \tag{3}$$

where β is a shape controlling parameter, $z_I = \|\boldsymbol{x} - \boldsymbol{x}_I\|$, and z_{mI} is the domain of influence of node I. The stationarity of $J(\boldsymbol{x})$ with respect to $\boldsymbol{a}(\boldsymbol{x})$ yields

$$\boldsymbol{A}(\boldsymbol{x})\boldsymbol{a}(\boldsymbol{x}) = \boldsymbol{C}(\boldsymbol{x})\boldsymbol{d}, \tag{4}$$

where

$$\boldsymbol{A}(\boldsymbol{x}) = \sum_{I=1}^{l} w_I(\boldsymbol{x})\boldsymbol{p}(\boldsymbol{x}_I)\boldsymbol{p}^T(\boldsymbol{x}_I) = \boldsymbol{P}^T\boldsymbol{W}\boldsymbol{P}, \tag{5}$$

and

$$\boldsymbol{C}(\boldsymbol{x}) = \left[w_1(\boldsymbol{x})\boldsymbol{p}(\boldsymbol{x}_1), \cdots, w_l(\boldsymbol{x})\boldsymbol{p}(\boldsymbol{x}_l)\right] = \boldsymbol{P}^T\boldsymbol{W}. \tag{6}$$

Solving for $\boldsymbol{a}(\boldsymbol{x})$ in Eq. (4) and then substituting into Eq. (1) yields

$$u^h(\boldsymbol{x}) = \sum_{I=1}^{l} \Phi_I(\boldsymbol{x}) d_I = \boldsymbol{\Phi}^T(\boldsymbol{x})\boldsymbol{d}, \tag{7}$$

where

$$\boldsymbol{\Phi}^T(\boldsymbol{x}) = \big\{\Phi_1(\boldsymbol{x}), \ldots, \Phi_l(\boldsymbol{x})\big\} = \boldsymbol{p}^T(\boldsymbol{x})\boldsymbol{A}^{-1}(\boldsymbol{x})\boldsymbol{C}(\boldsymbol{x}) \tag{8}$$

is a vector with its Ith component

$$\Phi_I(\boldsymbol{x}) = \sum_{j=1}^{m} p_j(\boldsymbol{x})\big[\boldsymbol{A}^{-1}(\boldsymbol{x})\boldsymbol{C}(\boldsymbol{x})\big]_{jI}, \tag{9}$$

representing the shape function of the MLS approximation corresponding to node I. The partial derivatives of $\Phi_I(\boldsymbol{x})$ can also be obtained as

$$\Phi_{I,i}(\boldsymbol{x}) = \sum_{j=1}^{m} \big\{p_{j,i}(\boldsymbol{A}^{-1}\boldsymbol{C})_{jI} + p_j(\boldsymbol{A}^{-1}_{,i}\boldsymbol{C} + \boldsymbol{A}^{-1}\boldsymbol{C}_{,i})_{jI}\big\}, \tag{10}$$

where $\boldsymbol{A}^{-1}_{,i} = -\boldsymbol{A}^{-1}\boldsymbol{A}_{,i}\boldsymbol{A}^{-1}$ and $()_{,i} = \partial()/\partial x_i$. From Eqs. (6) and (9), $\Phi_I(\boldsymbol{x}) = 0$ when $w_I(\boldsymbol{x}) = 0$. In other words, $\Phi_I(\boldsymbol{x})$ vanishes for $\boldsymbol{x}$ not in the support of nodal point $\boldsymbol{x}_I$, thus preserving the local character of the MLS approximation.

2.2. *Variational formulation and discretization*

For small displacements in two-dimensional, isotropic, and linear-elastic solids, the equilibrium equations and boundary conditions are

$$\boldsymbol{\nabla}\cdot\boldsymbol{\sigma} + \boldsymbol{b} = \boldsymbol{0} \quad \text{in } \mathcal{D} \text{ and} \tag{11}$$

$$\begin{array}{ll} \boldsymbol{\sigma}\cdot\boldsymbol{n} = \bar{\boldsymbol{t}} & \text{on } \Gamma_t \text{ (natural boundary conditions)} \\ \boldsymbol{u} = \bar{\boldsymbol{u}} & \text{on } \Gamma_u \text{ (essential boundary conditions)} \end{array}, \tag{12}$$

respectively, where $\boldsymbol{\sigma} = \boldsymbol{D}\boldsymbol{\varepsilon}$ is the stress vector, $\boldsymbol{D}$ is the material property matrix, $\boldsymbol{\varepsilon} = \boldsymbol{\nabla}_s\boldsymbol{u}$ is the strain vector, $\boldsymbol{u}$ is the displacement vector, $\boldsymbol{b}$ is the body force vector, $\bar{\boldsymbol{t}}$ and $\bar{\boldsymbol{u}}$ are the vectors of prescribed surface tractions and displacements, respectively, $\boldsymbol{n}$ is a unit normal to the domain $\mathcal{D}$, Γ_t and Γ_u are the portions of boundary Γ where tractions and displacements are respectively prescribed, $\boldsymbol{\nabla}^T = \{\partial/\partial x_1, \partial/\partial x_2\}$ is the vector of gradient operators, and $\boldsymbol{\nabla}_s\boldsymbol{u}$ is the symmetric part of $\boldsymbol{\nabla}\boldsymbol{u}$. The variational or weak form of Eqs. (11) and (12) is

$$\begin{aligned} &\int_{\mathcal{D}} \boldsymbol{\sigma}^T\boldsymbol{\delta\varepsilon}\,d\mathcal{D} - \int_{\mathcal{D}} \boldsymbol{b}^T\delta\boldsymbol{u}\,d\mathcal{D} - \int_{\Gamma} \bar{\boldsymbol{t}}^T\delta\boldsymbol{u}\,d\Gamma_t \\ &\quad + \sum_{x_k\in\Gamma_u} \boldsymbol{f}^T(\boldsymbol{x}_k)\delta\boldsymbol{u}(\boldsymbol{x}_k) + \sum_{x_k\in\Gamma_u} \delta f^T(\boldsymbol{x}_k)\big[\boldsymbol{u}(\boldsymbol{x}_k) - \bar{\boldsymbol{u}}(\boldsymbol{x}_k)\big] = 0, \end{aligned} \tag{13}$$

where $\boldsymbol{f}^T(\boldsymbol{x}_k)$ is the vector of reaction forces at the constrained node k on Γ_u and δ denotes the variation operator. From Eq. (7), the MLS approximation of $\boldsymbol{u}(\boldsymbol{x}) = \big\{u_1(\boldsymbol{x}), u_2(\boldsymbol{x})\big\}^T$ in two dimensions is

$$\boldsymbol{u}^h(\boldsymbol{x}) = \boldsymbol{\Phi}^T\boldsymbol{d}, \tag{14}$$

where

$$\boldsymbol{\Phi}^T(\boldsymbol{x}) = \begin{bmatrix} \Phi_1(\boldsymbol{x}) & 0 & \cdots & \Phi_M(\boldsymbol{x}) & 0 \\ 0 & \Phi_1(\boldsymbol{x}) & \cdots & 0 & \Phi_M(\boldsymbol{x}) \end{bmatrix}, \tag{15}$$

$\boldsymbol{d} = \{d_1^1, d_1^2, \ldots, d_M^1, d_M^2\}^T \in \mathbb{R}^{2M}$ is the vector of nodal parameters or generalized displacements, and M is the total number of nodal points in $\mathcal{D}$. Applying the MLS approximation of Eq. 14 to discretization of Eq. 13 yields a linear system of equilibrium equations

$$\boldsymbol{K}Y = \boldsymbol{F}, \tag{16}$$

or

$$\underbrace{\begin{bmatrix} \boldsymbol{k} & \boldsymbol{G} \\ \boldsymbol{G}^T & \boldsymbol{0} \end{bmatrix}}_{\boldsymbol{K}} \underbrace{\begin{Bmatrix} \boldsymbol{d} \\ \boldsymbol{f}_R \end{Bmatrix}}_{Y} = \underbrace{\begin{Bmatrix} \boldsymbol{f}^{\text{ext}} \\ \boldsymbol{g} \end{Bmatrix}}_{\boldsymbol{F}}, \tag{17}$$

where

$$\boldsymbol{k} = \begin{bmatrix} \boldsymbol{k}_{11} & \boldsymbol{k}_{12} & \cdots & \boldsymbol{k}_{1M} \\ \boldsymbol{k}_{21} & \boldsymbol{k}_{22} & \cdots & \boldsymbol{k}_{2M} \\ \vdots & \vdots & \vdots & \vdots \\ \boldsymbol{k}_{M1} & \boldsymbol{k}_{M2} & \cdots & \boldsymbol{k}_{MM} \end{bmatrix} \in \mathbb{L}\big(\mathbb{R}^{2M} \times \mathbb{R}^{2M}\big) \tag{18}$$

is the stiffness matrix with

$$\boldsymbol{k}_{IJ} = \int_{\mathcal{D}} \boldsymbol{B}_I^T \boldsymbol{D} \boldsymbol{B}_J d\mathcal{D} \in \mathbb{L}\big(\mathbb{R}^2 \times \mathbb{R}^2\big), \tag{19}$$

$$\boldsymbol{G}^T = \begin{bmatrix} \Phi_1(\boldsymbol{x}_1) & 0 & \cdots & \Phi_1(\boldsymbol{x}_M) & 0 \\ 0 & \Phi_1(\boldsymbol{x}_1) & \cdots & 0 & \Phi_1(\boldsymbol{x}_M) \\ \vdots & \vdots & \ddots & \vdots & \vdots \\ \Phi_L(\boldsymbol{x}_1) & 0 & \cdots & \Phi_L(\boldsymbol{x}_M) & 0 \\ 0 & \Phi_L(\boldsymbol{x}_1) & \cdots & 0 & \Phi_L(\boldsymbol{x}_M) \end{bmatrix} \tag{20}$$

is a matrix comprising shape function values of nodes at which the displacement boundary conditions are prescribed, L is the total number of nodes on Γ_u, $\boldsymbol{f}_R = \{\boldsymbol{f}(\boldsymbol{x}_{k_1}), \ldots, \boldsymbol{f}(\boldsymbol{x}_{k_L})\}^T \in \mathbb{R}^{2L}$ is the vector of reaction forces on Γ_u,

$$\boldsymbol{f}^{\text{ext}} = \int_{\mathcal{D}} \boldsymbol{\Phi}^T \boldsymbol{b} d\mathcal{D} + \int_{\Gamma_t} \boldsymbol{\Phi}^T \bar{\boldsymbol{t}} d\Gamma_t \in \mathbb{R}^{2M} \tag{21}$$

is the force vector, $\boldsymbol{g} = \{\bar{\boldsymbol{u}}(\boldsymbol{x}_{k_1}), \ldots, \bar{\boldsymbol{u}}(\boldsymbol{x}_{k_L})\}^T \in \mathbb{R}^{2L}$ is the vector of prescribed displacements on Γ_u, and

$$\boldsymbol{B}_I = \begin{bmatrix} \Phi_{I,1} & 0 \\ 0 & \Phi_{I,2} \\ \Phi_{I,2} & \Phi_{I,1} \end{bmatrix}. \tag{22}$$

To perform numerical integrations in Eqs. (19) and (21), a background mesh is required, which can be independent of the arrangement of meshfree nodes. However, in forthcoming numerical examples, the nodes of the background mesh coincide with the meshless nodes. Standard 4×4 Gaussian quadratures are used to evaluate the integrals for assembling the stiffness matrix and the force vector.

2.3. *Essential boundary conditions*

In solving for $\boldsymbol{d}$, the essential boundary conditions must be enforced. The lack of Kronecker delta properties in meshless shape functions presents some difficulty in imposing essential boundary conditions in EFGM. Nevertheless, several methods are currently available for enforcing essential boundary conditions. In this work, a full transformation method[12,25] is employed for stochastic applications.

It should be noted that the generalized displacement vector $\boldsymbol{d}$ represents the nodal parameters, and not the actual displacements at meshfree nodes. Let $\hat{\boldsymbol{d}} = \{\boldsymbol{u}^h(\boldsymbol{x}_1), \ldots, \boldsymbol{u}^h(\boldsymbol{x}_M)\}^T \in \mathbb{R}^{2M}$ represent the vector of nodal displacements. From Eq. (14)

$$\hat{\boldsymbol{d}} = \boldsymbol{\Lambda}\boldsymbol{d}, \tag{23}$$

where $\boldsymbol{\Lambda} = [\boldsymbol{\Phi}^T(\boldsymbol{x}_1), \ldots, \boldsymbol{\Phi}^T(\boldsymbol{x}_M)]^T \in \mathbb{L}\big(\mathbb{R}^{2M} \times \mathbb{R}^{2M}\big)$ is the transformation matrix. Hence, $\hat{\boldsymbol{d}}$ can be easily calculated when $\boldsymbol{d}$ is known.

In summary, shape functions and resultant matrix equilibrium equations have been created without using any structured mesh, a key advantage of meshfree methods over FEM. However, the computational effort in generating these matrix equations is typically higher than that required by low-order FEM. Therefore, breakthrough research focused on enhancing speed and robustness of meshfree methods is required for their effective implementation.

3. Random Field and Parameterization

3.1. *Karhunen-Loève representation*

Let $(\Omega, \mathcal{F}, P)$ be a probability space, where Ω is the sample space, $\mathcal{F}$ is the σ-algebra of subsets of Ω and P is the probability measure. Defined on the probability space and indexed by a spatial coordinate $\boldsymbol{x} \in \mathcal{D} \subset \mathbb{R}^K, K = 1, 2,$ or 3, consider a real-valued random field $\alpha(\boldsymbol{x})$ with mean *zero* and covariance function $\Gamma(\boldsymbol{x}_1, \boldsymbol{x}_2) \equiv \mathbb{E}\big[\alpha(\boldsymbol{x}_1)\alpha(\boldsymbol{x}_2)\big]$, which is continuous over $\mathcal{D}$. Denote by $\mathcal{L}_2(\Omega, \mathcal{F}, P)$ or simply $\mathcal{L}_2$ a collection of random variables α for each $\boldsymbol{x} \in \mathcal{D}$ such that $\mathbb{E}[|\alpha|^2] < \infty$, where $\mathbb{E}$ represents the expectation operator. If α is in $\mathcal{L}_2$, then $\Gamma(\boldsymbol{x}_1, \boldsymbol{x}_2)$ is square integrable and hence a bounded function.

Let $\{\lambda_i, f_i(\boldsymbol{x})\}, i = 1, 2, \ldots, \infty$, be the eigenvalues and eigenfunctions of $\Gamma(\boldsymbol{x}_1, \boldsymbol{x}_2)$, which satisfy the integral equation[26]

$$\int_{\mathcal{D}} \Gamma(\boldsymbol{x}_1, \boldsymbol{x}_2) f_i(\boldsymbol{x}_2) d\boldsymbol{x}_2 = \lambda_i f_i(\boldsymbol{x}_1), \quad \forall i = 1, 2, \ldots, \infty. \tag{24}$$

The eigenfunctions are orthogonal in the sense that

$$\int_{\mathcal{D}} f_i(\boldsymbol{x}) f_j(\boldsymbol{x}) dx = \boldsymbol{\delta}_{ij}, \quad \forall i, j = 1, 2, \ldots, \infty, \tag{25}$$

with δ_{ij} representing the Kronecker delta. The Karhunen-Loève (K-L) representation of $\alpha(\boldsymbol{x})$ is[26]

$$\alpha(\boldsymbol{x}) = \sum_{i=1}^{\infty} V_i \sqrt{\lambda_i} f_i(\boldsymbol{x}), \tag{26}$$

where $V_i, i = 1, \ldots, \infty$ is an infinite sequence of uncorrelated random variables, each of which has *zero* mean and *unit* variance. In practice, the infinite series of Eq. (26) must be truncated, yielding a K-L approximation or expansion

$$\hat{\alpha}_M(\boldsymbol{x}) = \sum_{i=1}^{N} V_i \sqrt{\lambda_i} f_i(\boldsymbol{x}), \tag{27}$$

which approaches $\alpha(\boldsymbol{x})$ in the mean square sense for $\boldsymbol{x} \in \mathcal{D}$ as $N \to \infty$. According to Eq. (27), the K-L expansion provides a parametric representation of a random field with N random variables.

3.2. *Gaussian and translation random fields*

The K-L approximation captures only the second-moment properties of a random field. Hence, a random field that is completely described by its second-moment properties, such as a Gaussian random field, can be effectively approximated by K-L expansion. For example, if a random field is Gaussian, its K-L approximation in Eq. (27) forms a *zero*-mean, independent sequence of standard Gaussian random variables V_i, $i = 1, \ldots, N$. For a general non-Gaussian field, K-L representation cannot provide complete characterization and therefore may not be applicable. However, one class of non-Gaussian random fields for which the use of K-L expansion can be readily exploited is the class of translation random fields, where a non-Gaussian random field is defined as a nonlinear, memoryless transformation of a Gaussian random field.[27]

Let $Z(\boldsymbol{x})$ be a homogenous, non-Gaussian translation random field with mean μ_Z, standard deviation σ_Z, covariance function $\Gamma_Z(\boldsymbol{\xi}) \equiv \mathbb{E}[(Z(\boldsymbol{x}) - \mu_Z)(Z(\boldsymbol{x}+\boldsymbol{\xi}) - \mu_Z)]$, and marginal distribution F that has no atoms, and let $\alpha(\boldsymbol{x})$ be a homogeneous, *zero*-mean, Gaussian random field with *unit* variance and covariance function $\Gamma_\alpha(\boldsymbol{\xi}) \equiv \mathbb{E}[\alpha(\boldsymbol{x})\alpha(\boldsymbol{x}+\boldsymbol{\xi})]$. If G is a real-valued, monotonic, differentiable function, then,

$$Z(\boldsymbol{x}) = G[\alpha(\boldsymbol{x})] \tag{28}$$

can be viewed as a memoryless transformation of the Gaussian image field $\alpha(\boldsymbol{x})$. From the condition that the marginal distribution and the covariance function of $Z(\boldsymbol{x})$ coincide with specified target functions F and Γ_Z, respectively, it can be shown that[28,29]

$$G(\alpha) = F^{-1}[\Phi(\alpha)], \tag{29}$$

and

$$\mu_Z^2 + \Gamma_Z(\boldsymbol{\xi}) = \int_\infty^\infty \int_\infty^\infty (G(\alpha_1) - \mu_z)(G(\alpha_2) - \mu_z)\phi_2(\alpha_1, \alpha_2, \Gamma_\alpha(\boldsymbol{\xi}))d\alpha_1 d\alpha_2, \quad (30)$$

where Φ is the distribution function of a standard Gaussian variable and $\phi_2(\alpha_1, \alpha_2, \Gamma_\alpha(\boldsymbol{\xi}))$ is the bivariate standard Gaussian density function with correlation coefficient Γ_α. For given μ_Z, $\Gamma_Z(\boldsymbol{\xi})$, and F, G can be calculated from Eq. (29) and the required covariance function $\Gamma_\alpha(\boldsymbol{\xi})$ of $\alpha(\boldsymbol{x})$ can be solved from Eq. (30), if the target scaled covariance function $\Gamma_Z(\boldsymbol{\xi})/\Gamma_Z(\mathbf{0})$ is in the range $(\bar{\Gamma}^*, 1)$, where[29]

$$\bar{\Gamma}^* = \frac{\mathbb{E}\left[G(\alpha)G(-\alpha)\right] - \mathbb{E}\left[G(\alpha)\right]^2}{\mathbb{E}\left[G(\alpha)^2\right] - \mathbb{E}\left[G(\alpha)\right]^2}. \quad (31)$$

Once $\Gamma_\alpha(\boldsymbol{\xi})$ is determined, the parameterization of $Z(\boldsymbol{x})$ is achieved by K-L expansion of its Gaussian image, i.e.

$$Z(\boldsymbol{x}) \simeq G\left[\sum_{i=1}^N V_i \sqrt{\lambda_i} f_i(\boldsymbol{x})\right], \quad (32)$$

where V_i, $i = 1, \ldots, N$ are independent standard Gaussian random variables, and $\{\lambda_i, f_i(\boldsymbol{x})\}$, $i = 1, \ldots, N$ are eigenvalues and eigenfunctions of $\Gamma_\alpha(\boldsymbol{\xi})$.

3.3. *Meshfree method for solving integral equation*

The K-L expansion requires solution of an integral eigenvalue problem (Eq. (24)), which is not an easy task in general. Closed-form solutions are only available when the covariance kernel has simpler functional forms, such as exponential and linear functions, or domain $\mathcal{D}$ is rectangular. For arbitrary covariance functions or arbitrary domains, numerical methods are often needed to solve the eigenvalue problem. In this section, meshfree shape functions from EFGM are employed to solve the eigenvalue problem.[18]

For a random field $\alpha(\boldsymbol{x})$ indexed by $\boldsymbol{x} \in \mathcal{D} \subset \mathbb{R}^K$, $K = 1, 2,$ or 3, consider an MLS approximation of the eigenfunction $f_i(\boldsymbol{x})$, given by

$$f_i(\boldsymbol{x}) = \sum_{I=1}^M \hat{f}_{iI} \Phi_I(\boldsymbol{x}), \quad (33)$$

where $\hat{f}_{iI}$ is the Ith nodal parameter for the ith eigenfunction, $\Phi_I(\boldsymbol{x})$ is the meshless shape function of the Ith node (see Sec. 2), and M is the total number of nodes. Hence, Eq. (24) becomes

$$\sum_{I=1}^M \hat{f}_{iI} \int_{\mathcal{D}} \Gamma(\boldsymbol{x}_1 \boldsymbol{x}_2)\Phi_I(\boldsymbol{x}_2)d\boldsymbol{x}_2 - \lambda_i \sum_{I=1} \hat{f}_{iI}\Phi_I(\boldsymbol{x}_1). \quad (34)$$

Define

$$\varepsilon_M = \sum_{I=1}^M \hat{f}_{iI}\left(\int_{\mathcal{D}} \Gamma(\boldsymbol{x}_1, \boldsymbol{x}_2)\Phi_I(\boldsymbol{x}_2)\boldsymbol{d}\boldsymbol{x}_2 - \lambda_i \Phi_I(\boldsymbol{x}_1)\right) \quad (35)$$

as the residual error, which is associated with meshless discretization involving an M number of nodes. Following Galerkin approximation,

$$\int_{\mathcal{D}} \varepsilon_M \Phi_J(\boldsymbol{x}_1) d\boldsymbol{x}_1 = 0, \quad \forall J = 1, \ldots, M, \tag{36}$$

which, when combined with Eq. (35) can be expanded to yield the following matrix equation

$$\lambda_i \boldsymbol{R} \hat{\boldsymbol{f}}_i = \boldsymbol{S} \hat{\boldsymbol{f}}_i, \tag{37}$$

where $\hat{\boldsymbol{f}}_i = \{\hat{f}_{i1}, \ldots, \hat{f}_{iM}\}^T$ is the ith eigenvector, $\boldsymbol{R} = [R_{IJ}]$, $\boldsymbol{S} = [S_{IJ}]$,

$$R_{IJ} = \int_{\mathcal{D}} \int_{\mathcal{D}} \Gamma(\boldsymbol{x}_1, \boldsymbol{x}_2) \Phi_I(\boldsymbol{x}_2) \Phi_J(\boldsymbol{x}_1) d\boldsymbol{x}_1 d\boldsymbol{x}_2, \quad \forall I, J = 1 \ldots, M, \tag{38}$$

and

$$S_{IJ} = \int_{\mathcal{D}} \Phi_I(\boldsymbol{x}) \Phi_J(\boldsymbol{x}) d\boldsymbol{x}, \quad \forall I, J = 1, \ldots, M. \tag{39}$$

Equation (37) represents the matrix analog of the integral eigenvalue problem for a multi-dimensional random field with an arbitrary domain. Equation (37) can be formulated for any covariance function or domain and can be easily solved by standard methods. Hence, the meshfree method can solve problems involving a multi-dimensional random field with an arbitrary covariance function and an arbitrary domain. Once the eigenvector $\hat{\boldsymbol{f}}_i$ is calculated, Eq. (33) can be used to determine the eigenfunction $f_i(\boldsymbol{x})$.

Note that the meshless discretization proposed here is only intended for solving the integral eigenvalue problem, not for discretizing the random field. Matrices $\boldsymbol{R}$ and $\boldsymbol{S}$, which involve $2K$- and K-dimensional integration, respectively, can be computed using standard numerical quadrature. Integration involves meshless shape functions, which are already calculated and stored for meshless stress analysis. Hence, matrices $\boldsymbol{R}$ and $\boldsymbol{S}$ can be generated with little extra effort. However, for a large K, the computational effort in performing numerical integration can become intensive. Also note that for meshless stress analysis it is not necessary that the number and spatial distribution of nodes coincide with those for eigenfunction approximation. Different and selective discretizations can be employed, if necessary. However, in this study the same discretization is used for both meshless stress analysis and for solving the eigenvalue problem.

3.4. *Example 1: Eigensolution for a two-dimensional domain*

Consider a two-dimensional domain $\mathcal{D}$ that is constructed by subtracting a quarter of a circle of radius $a = 1$ unit from a square of size $L = 20$ units, as depicted by Fig. 2. A homogeneous Gaussian random field $\alpha(\boldsymbol{x})$ defined over $\mathcal{D}$ has mean *zero* and a bounded covariance function

$$\Gamma_\alpha(\boldsymbol{\xi}) = \sigma_\alpha^2 \exp\left(-\frac{\|\boldsymbol{\xi}\|}{bL}\right), \quad \forall \boldsymbol{x}, \boldsymbol{x} + \boldsymbol{\xi} \in \mathcal{D}, \tag{40}$$

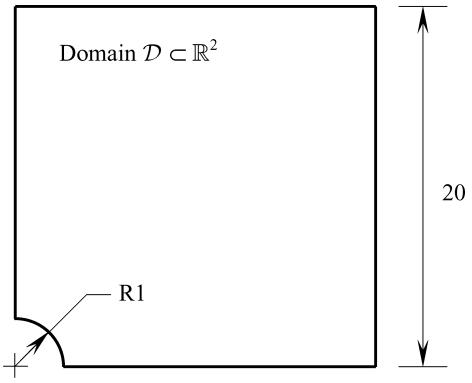

Fig. 2. A two-dimensional domain $\mathcal{D}$ for random field $\alpha(\boldsymbol{x}), \boldsymbol{x} \in \mathcal{D} \subset \mathbb{R}^2$.

where $\sigma_\alpha = 0.1$ unit and $b = 0.5$. Since the domain is not rectangular, no analytical solution of eigenvalues and eigenfunctions exists for the above covariance function. Therefore, the meshfree method is needed to find a numerical solution. Figures 3(a) though 3(e) show five meshfree discretizations of $\mathcal{D}$ with total number of nodes $M = 9, 20, 30, 56$, and 90, respectively, which represent progressively increasing degrees of refinement.[18]

Figure 4 shows several eigenvalues calculated using the meshfree method (Eqs. 33–39) for $M = 9, 20, 30, 56$, and 90, for the given covariance kernel. Clearly, the eigenvalues converge with respect to M, as expected. Similar comparisons of the first four eigenfunctions $f_1(\boldsymbol{x})$, $f_2(\boldsymbol{x})$, $f_3(\boldsymbol{x})$, and $f_4(\boldsymbol{x})$, presented in Figs. 5(a), 5(b),

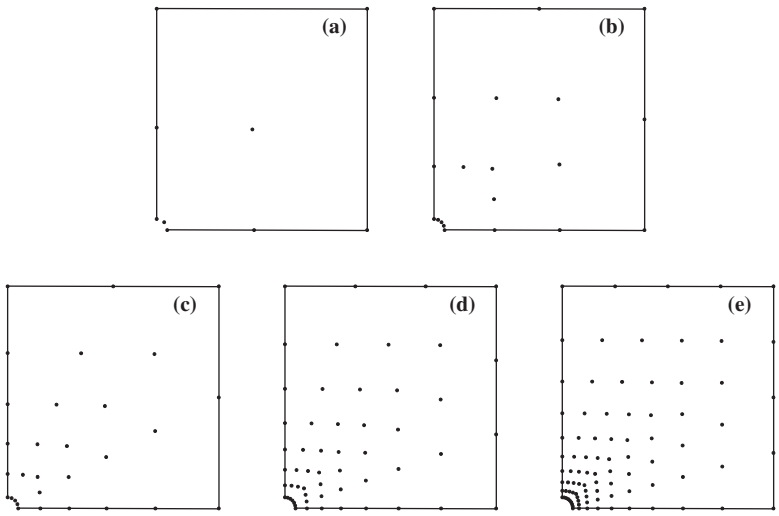

Fig. 3. Various meshfree discretizatons; (a) $M = 9$; (b) $M = 20$; (c) $M = 30$; (d) $M = 56$; (e) $M = 90$.[18]

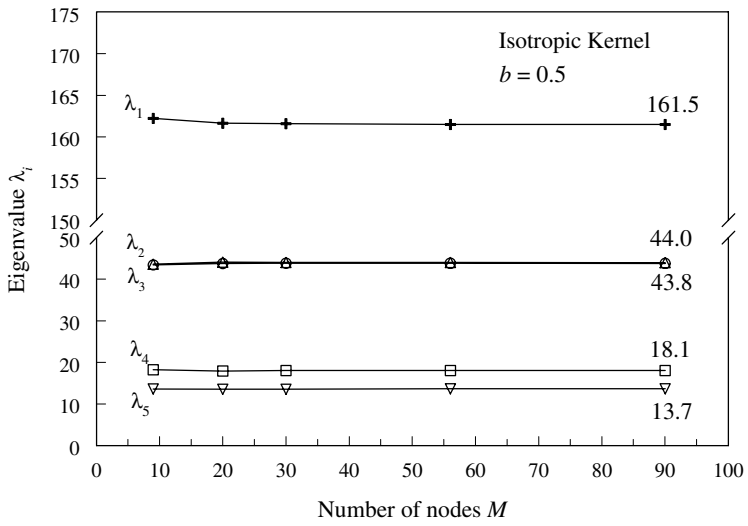

Fig. 4. Eigenvalues for various meshfree discretizations.[18]

6(a), and 6(b), respectively, also demonstrate the convergence of eigenfunctions with respect to M. These convergent solutions of eigenvalues and eigenfunctions provide confidence in the following probabilistic results.

4. Multivariate Function Decomposition

Consider a continuous, differentiable, real-valued multivariate function $y(\boldsymbol{v})$ that depends on $\boldsymbol{v} = \{v_1, \cdots, v_N\}^T \in \mathbb{R}^N$. Suppose, $y(\boldsymbol{v})$ has a convergent Taylor expansion at an arbitrary reference point $\boldsymbol{c} = \{c_1, \cdots, c_N\}^T$. Applying the Taylor series expansion of $y(\boldsymbol{v})$ at $\boldsymbol{v} = \boldsymbol{c}$, $y(\boldsymbol{v})$ can be expressed by

$$y(\boldsymbol{v}) = y(\boldsymbol{c}) + \sum_{j=1}^{\infty} \frac{1}{j!} \sum_{i=1}^{N} \frac{\partial^j y}{\partial v_i^j}(\boldsymbol{c})(v_i - c_i)^j + R_2, \tag{41}$$

or

$$\begin{aligned} y(\boldsymbol{v}) = y(c) &+ \sum_{j=1}^{\infty} \frac{1}{j!} \sum_{i=1}^{N} \frac{\partial^j y}{\partial v_i^j}(\boldsymbol{c})(v_i - c_i)^j \\ &+ \sum_{j_1, j_2 > 0}^{\infty} \frac{1}{j_1! j_2!} \sum_{i_1 < i_2} \frac{\partial^{j_1 + j_2} y}{\partial v_{i_1}^{j_1} \partial v_{i_2}^{j_2}}(\boldsymbol{c})(v_{i_1} - c_{i_1})^{j_1}(v_{i_2} - c_{i_2})^{j_2} + R_3, \end{aligned} \tag{42}$$

where the remainder R_2 denotes all terms with dimension two and higher and the remainder R_3 denotes all terms with dimension three and higher.

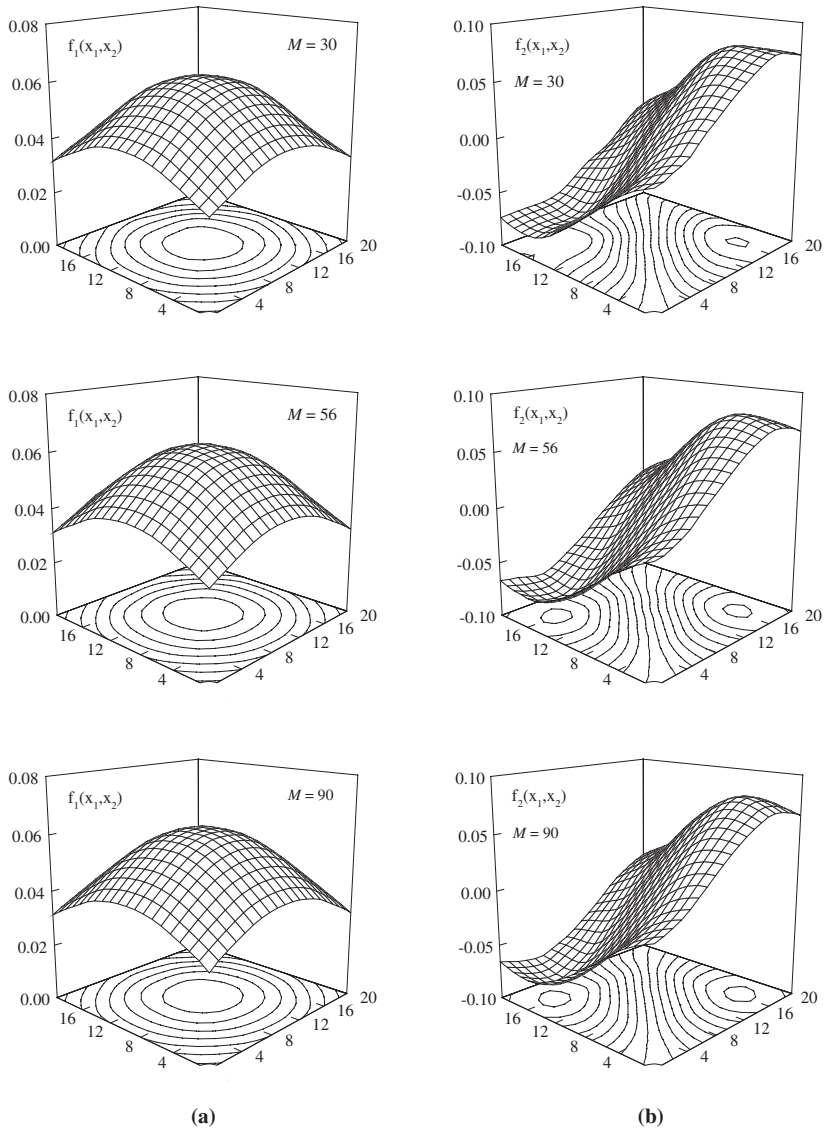

Fig. 5. First and second eigenfunctions by meshfree method; (a) $f_1(\boldsymbol{x})$; (b) $f_2(\boldsymbol{x})$.[18]

4.1. *Univariate approximation*

Consider a univariate approximation of $y(\boldsymbol{v})$, denoted by

$$\hat{y}_1(\boldsymbol{v}) \equiv \hat{y}_1(v_1, \ldots, v_N) = \sum_{i=1}^{N} y(c_1, \ldots, c_{i-1}, v_i, c_{i+1}, \ldots, c_N) - (N-1)y(\boldsymbol{c}), \quad (43)$$

where each term in the summation is a function of only one variable and can be subsequently expanded in a Taylor series at $\boldsymbol{v} = \boldsymbol{c}$ yielding

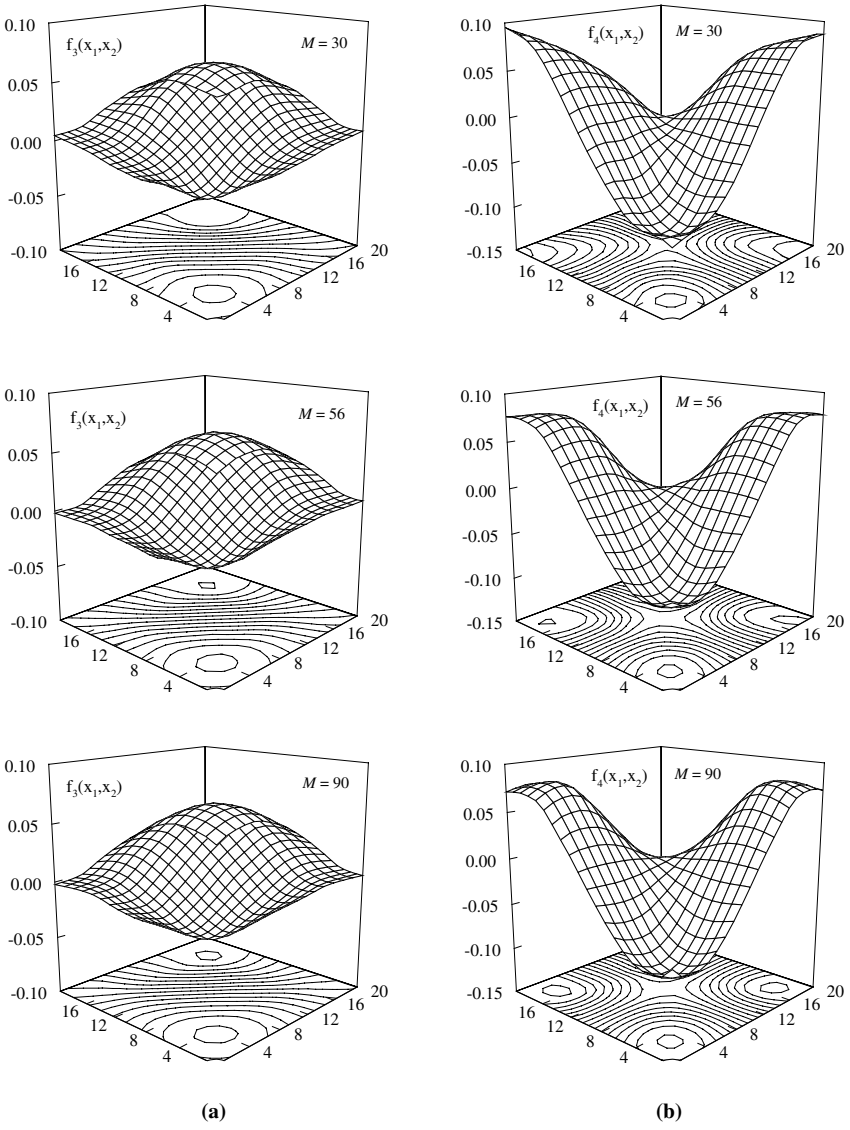

Fig. 6. Third and fourth eigenfunctions by meshfree method; (a) $f_3(\boldsymbol{x})$; (b) $f_4(\boldsymbol{x})$.[18]

$$\hat{y}_1(\boldsymbol{v}) = y(\boldsymbol{c}) + \sum_{j=1}^{\infty} \frac{1}{j!} \sum_{i=1}^{N} \frac{\partial^j y}{\partial v_i^j}(\boldsymbol{c})(v_i - c_i)^j. \tag{44}$$

Comparison of Eqs. (41) and (44) indicates that the univariate approximation leads to the residual error $y(\boldsymbol{v}) - \hat{y}_1(\boldsymbol{v}) = R_2$, which includes contributions from terms of dimension two and higher. For a sufficiently smooth $y(\boldsymbol{v})$ having a convergent Taylor series, the coefficients associated with higher-dimensional terms are usually

much smaller than those associated with one-dimensional terms. As such, higher-dimensional terms contribute less to the function, and therefore, can be neglected. Furthermore, Eq. (43) exactly represents $y(\boldsymbol{v}) = \sum y_i(v_i)$, i.e. when $y(\boldsymbol{v})$ can be additively decomposed into functions $y_i(x_i)$ of single variables.

4.2. *Bivariate approximation*

In a similar manner, consider a bivariate approximation

$$\hat{y}_2(\boldsymbol{v}) = \sum_{i_1<i_2} y(c_1,\ldots,c_{i_1-1},v_{i_1},c_{i_1+1},\ldots,c_{i_2-1},v_{i_2},c_{i_2+1},\ldots,c_N) - (N-2)\sum_{i=1}^{N} y(c_1,\ldots,c_{i-1},v_i,c_{i+1},\ldots,c_N) + \frac{(N-1)(N-2)}{2} y(\boldsymbol{c}) \quad (45)$$

of $y(\boldsymbol{v})$, where each term on the right hand side is a function of at most two variables and can be expanded in a Taylor series at $\boldsymbol{v} = \boldsymbol{c}$, yielding

$$\hat{y}_2(\boldsymbol{v}) = y(\boldsymbol{c}) + \sum_{j=1}^{\infty}\frac{1}{j!}\sum_{i=1}^{N}\frac{\partial^j y}{\partial v_i^j}(\boldsymbol{c})(v_i-c_i)^j + \sum_{j_1,j_2>0}^{\infty}\frac{1}{j_1!j_2!}\sum_{i_1<i_2}\frac{\partial^{j_1+j_2} y}{\partial v_{i_1}^{j_1}\partial v_{i_2}^{j_2}}(\boldsymbol{c})(v_{i_1}-c_{i_1})^{j_1}(v_{i_2}-c_{i_2})^{j_2}. \quad (46)$$

Again, the comparison of Eqs. (42) and (46) indicates that the bivariate approximation leads to the residual error $y(\boldsymbol{v}) - \hat{y}_2(\boldsymbol{v}) = R_3$, in which the remainder R_3 includes terms of dimension three and higher. The bivariate approximation includes all terms with no more than two variables, thus yielding higher accuracy than the univariate approximation. Furthermore, Eq. (45) exactly represents $y(\boldsymbol{v}) = \sum\sum y_{ij}(v_i, v_j)$, i.e. when $y(\boldsymbol{v})$ can be additively decomposed into functions $y_{ij}(v_i, v_j)$ of at most two variables.

4.3. *Generalized S-variate approximation*

The procedure for univariate and bivariate approximations described in the preceding can be generalized to an S-variate approximation for any integer $1 \le S \le N$. The generalized S-variate approximation of $y(\boldsymbol{v})$ is[22–24]

$$\hat{y}_S(\boldsymbol{v}) \equiv \sum_{i=0}^{S}(-1)^i \binom{N-S+i-1}{i} y_{S-i}(\boldsymbol{v}), \quad (47)$$

where

$$y_R = \sum_{k=0}^{R}\binom{N-k}{R-k} t_k; \quad 0 \le R \le S, \quad (48)$$

with

$$
\begin{aligned}
t_0 &= y(\boldsymbol{c}) \\
t_1 &= \sum_{j_1} \frac{1}{j_1!} \sum_{i_1=1}^{N} \frac{\partial^{j_1} y}{\partial v_{i_1}^{j_1}}(\boldsymbol{c}) \left(v_{i_1} - c_{i_1}\right)^{j_1} \\
t_2 &= \sum_{j_1,j_2} \frac{1}{j_1! j_2!} \sum_{i_1<i_2} \frac{\partial^{j_1+j_2} y}{\partial v_{i_1}^{j_1} \partial v_{i_2}^{j_2}}(\boldsymbol{c}) \left(v_{i_1} - c_{i_1}\right)^{j_1} \left(v_{i_2} - c_{i_2}\right)^{j_2} \\
&\vdots \\
t_S &= \sum_{j_1,\ldots,j_S} \frac{1}{j_1! \cdots j_S!} \sum_{i_1<\cdots<i_S} \frac{\partial^{j_1+\cdots+j_S} y}{\partial v_{i_1}^{j_1} \cdots \partial v_{i_S}^{j_S}}(\boldsymbol{c}) \left(v_{i_1} - c_{i_1}\right)^{j_1} \cdots \left(v_{i_S} - c_{i_S}\right)^{j_S}.
\end{aligned}
\tag{49}
$$

Using a multivariate function decomposition theorem, developed by the author's group, it can be shown that $\hat{y}_S(\boldsymbol{v})$ in Eq. (47) consists of all terms of the Taylor series of $y(\boldsymbol{v})$ that have less than or equal to S variables.[23] The expanded form of Eq. (47), when compared with the Taylor expansion of $y(\boldsymbol{v})$, indicates that the residual error in the S-variate approximation is $y(\boldsymbol{v}) - \hat{y}_S(\boldsymbol{v}) = R_{S+1}$, where the remainder R_{S+1} includes terms of dimension $S+1$ and higher. When $S = 1$, Eq. (47) degenerates to the univariate approximation (Eq. (43)). When $S = 2$, Eq. (47) becomes the bivariate approximation (Eq. (45)). Similarly, trivariate, quadrivariate, and other higher-variate approximations can be derived by appropriately selecting the value of S. In the limit, when $S = N$, Eq. (47) converges to the exact function $y(\boldsymbol{v})$. In other words, the decomposition technique generates a convergent sequence of approximations of $y(\boldsymbol{v})$.

5. Statistical Moment Analysis

5.1. *General stochastic response*

Consider a mechanical system subject to a *zero*-mean independent random input vector $\boldsymbol{V} = \{V_1, \ldots, V_N\}^T \in \mathbb{R}^N$, which characterizes uncertainty in loads, material properties, and geometry. Let $g(\boldsymbol{V})$ represent a general stochastic response of interest, for which the lth statistical moment

$$
m_l \equiv \mathbb{E}\left[g^l(\boldsymbol{V})\right] = \int_{\mathbb{R}^N} g^l(\boldsymbol{v}) f_{\boldsymbol{V}}(\boldsymbol{v}) d\boldsymbol{v} \tag{50}
$$

is sought, where $f_{\boldsymbol{V}}(\boldsymbol{v})$ is the joint probability density function of $\boldsymbol{V}$. If $y(\boldsymbol{V}) = g^l(\boldsymbol{V})$, the lth moment can also be evaluated from

$$
m_l = \mathbb{E}[y(\boldsymbol{V})] = \int_{\mathbb{R}^N} y(\boldsymbol{v}) f_{\boldsymbol{V}}(\boldsymbol{v}) d\boldsymbol{v}. \tag{51}
$$

Following the S-variate approximation procedure discussed in Eqs. (47)–(49) and using $\boldsymbol{c} = 0$ (mean input),

$$m_l \cong \mathbb{E}\left[\hat{y}_S(\boldsymbol{V})\right] = \sum_{i=0}^{S} (-1)^i \binom{N-S+i-1}{i} \times \sum_{k_1<k_2<\cdots<k_{S-i}} \mathbb{E}\big[y\big(0,\ldots,0,V_{k_1},0,\ldots,0,V_{k_2},0,\ldots,0,V_{k_{S-i}},0,\ldots,0\big)\big]. \tag{52}$$

If $f_{V_{k_j}}(v_{k_j})$ represents the marginal density of V_{k_j}, then by definition

$$\mathbb{E}\big[y\big(0,\ldots,0,V_{k_1},0,\ldots,0,V_{k_2},0,\ldots,0,V_{k_{S-i}},0,\ldots,0\big)\big] \equiv \int_{-\infty}^{\infty} y\big(0,\ldots,0,v_{k_1},0,\ldots,0,v_{k_2},0,\ldots,0,v_{k_{S-i}},0,\ldots,0\big) \prod_{j=1}^{S-i} f_{V_{k_j}}(v_{k_j}) dv_{k_j}, \tag{53}$$

which is valid for any independent random vector $\boldsymbol{V}$. If $\boldsymbol{V}$ comprises dependent variables, an appropriate transformation, such as the Rosenblatt transformation,[30] should be applied to map the dependent random vector $\boldsymbol{V}$ to an independent standard Gaussian random vector $\boldsymbol{U}$. Note that Eq. (53) only requires at most S-dimensional deterministic integration, which can be more easily evaluated using standard quadrature rules if $S \ll N$. For example, Gauss-Legendre and Gauss-Hermite quadratures are frequently used when V_j follows uniform and Gaussian distributions, respectively.[31] For an arbitrary distribution of V_j, a moment-based quadrature rule developed by the author can be used to evaluate the integral.[23]

The moment equation entails evaluating at most S-dimensional integrals, which is substantially simpler and more efficient than performing one N-dimensional integration when $S \ll N$. For practical problems involving a large number of input random variables (e.g. $N > 30$), the moment equation presents a promising method. The method does not require calculation of any partial derivatives of response and inversion of random matrices as compared with, respectively, the commonly used Taylor/perturbation and Neumann expansion methods. Hence, the computation effort in conducting statistical moment analysis is significantly reduced using the function decomposition technique. The method is coined "*S-variate* or *multivariate dimension-reduction method*," since calculation of an N-dimensional integral is essentially reduced to that of an at most S-dimensional integral.[23] When $S = 1$, the method degenerates to the *univariate dimension-reduction method* involving only one-dimensional integrations.[22] When $S = 2$, the method becomes the *bivariate dimension-reduction method* entailing at most two-dimensional integrations. Similarly, trivariate, quadrivariate, and other higher-variate methods can be derived by appropriately selecting the value of S. In the limit, when $S = N$, there is no dimension reduction and the method yields the exact solution.

5.2. *Discrete equilibrium equations*

Consider a linear mechanical system subject to a vector of input random parameters $\boldsymbol{V} \in \mathbb{R}^N \mapsto (\boldsymbol{\mu}, \boldsymbol{\gamma})$ characterizing uncertainty in the system and loads. Following

discretization, let $\boldsymbol{Y} \in \mathbb{R}^L \mapsto \left(\boldsymbol{m}_{\boldsymbol{Y}}, \boldsymbol{\gamma}_{\boldsymbol{Y}}\right)$ represent a displacement (response) vector associated with L degrees of freedom of the system, satisfying the linear equilibrium equation

$$\boldsymbol{K}(\boldsymbol{V})\boldsymbol{Y}(\boldsymbol{V}) = \boldsymbol{F}(\boldsymbol{V}), \tag{54}$$

in which the stiffness matrix $\boldsymbol{K}$ and force vector $\boldsymbol{F}$ depend on $\boldsymbol{V}$ and were defined in Sec. 2 in the review of meshfree formulation for linear elasticity. Equation (54) is common in mesh-free methods when the system, loads, or both, are uncertain. The solution

$$\boldsymbol{Y}(\boldsymbol{V}) = \boldsymbol{K}(\boldsymbol{V})^{-1}\boldsymbol{F}(\boldsymbol{V}) \tag{55}$$

is random and depends on $\boldsymbol{V}$. Using the S-variate dimension-reduction method, the mean vector $\boldsymbol{m}_{\boldsymbol{Y}}$ and covariance matrix $\boldsymbol{\gamma}_{\boldsymbol{Y}}$ of $\boldsymbol{Y}$ can be derived as

$$\boldsymbol{m}_{\boldsymbol{Y}} \cong \mathbb{E}[\hat{\boldsymbol{Y}}] = \sum_{i=0}^{S} (-1)^i \binom{N-S+i-1}{i} \sum_{k_1<k_2<\cdots<k_{S-i}} \mathbb{E}\left[\boldsymbol{K}(\tilde{\boldsymbol{V}}_i)^{-1}\boldsymbol{F}(\tilde{\boldsymbol{V}}_i)\right], \tag{56}$$

$$\boldsymbol{\gamma}_{\boldsymbol{Y}} = \mathbb{E}\left[\boldsymbol{Y}\boldsymbol{Y}^T\right] - \boldsymbol{m}_{\boldsymbol{Y}}\boldsymbol{m}_{\boldsymbol{Y}}^T, \tag{57}$$

where $\tilde{\boldsymbol{V}}_i = \{0, \ldots, 0, V_{k_1}, 0, \ldots, 0, V_{k_{S-i}}, 0, \ldots, 0\}^T$ and

$$\mathbb{E}\big[\boldsymbol{Y}\boldsymbol{Y}^T\big] \cong \sum_{i=0}^{S} (-1)^i \binom{N-S+i-1}{i} \times \sum_{k_1<k_2<\ldots<k_{S-i}} \mathbb{E}\left[\boldsymbol{K}(\tilde{\boldsymbol{V}}_i)^{-1}\boldsymbol{F}(\tilde{\boldsymbol{V}}_i)\boldsymbol{F}(\tilde{\boldsymbol{V}}_i)^T\boldsymbol{K}(\tilde{\boldsymbol{V}}_i)^{-T}\right]. \tag{58}$$

Note that the calculation of expected values on the right hand side of Eqs. (56)–(58) involves at most S-dimensional integrations.

5.3. *Example 2: Response statistics of a plate with a hole*

Consider a square plate with a circular hole, as shown in Fig. 7. The plate has dimension $2L = 40$ units, a hole with diameter $2a = 2$ units, and is subjected to a far-field, uniformly distributed stress of magnitude $\sigma^\infty = 1$ unit. The Poisson's ratio $\nu = 0.3$. The elastic modulus is a homogeneous Gaussian random field $E(\boldsymbol{x}) = \mu_E[1 + \alpha(\boldsymbol{x})]$; $\boldsymbol{x} \in \mathcal{D} \subset \mathbb{R}^2$, where $\mu_E = 1$ unit is the constant mean over domain $\mathcal{D}$ and $\alpha(\boldsymbol{x})$ is a homogeneous Gaussian random field with mean *zero* and covariance function defined by Eq. (40) in Example 1.[a] Furthermore, the modulus of elasticity is assumed to be symmetrically distributed with respect to x_1- and x_2-axes (see Fig. 7). Therefore, only a quarter of the plate needs to be analyzed.

[a]The Gaussian random field is adopted in Example 2 to allow direct comparison between dimension-reduction methods and Neumann expansion method,[32] of which the latter method entails the Gaussian assumption. The dimension-reduction methods do not require any specific distribution of random fields or variables.[23]

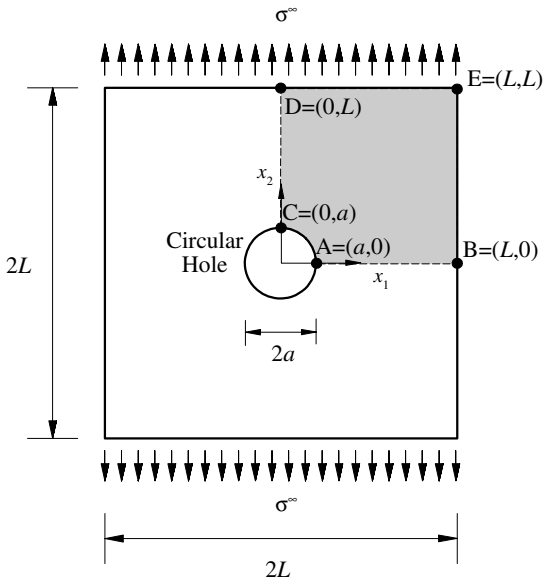

Fig. 7. A square plate with a hole subjected to uniform tension.

Figures 3(a)–3(e) show several meshfree discretizations of the quarter plate with various degrees of refinement. A plane stress condition is assumed.

Based on the correlation parameter $b = 0.5$, a value of $N = 12$ was selected for the K-L approximation of $\alpha(\boldsymbol{x})$. The meshfree method using the finest discretization (i.e. $M = 90$; see Fig. 3(e) in Example 1) was employed to obtain both the stress field and eigensolutions $\{\lambda_j, \phi_j(\boldsymbol{x})\}$, $j = 1, \ldots, 12$. Hence, the input random vector $\boldsymbol{V} = \{V_1, \ldots, V_{12}\}^T$ becomes a twelve-dimensional standard Gaussian random vector.

Table 1 presents standard deviations of displacements and strains at points A, B, C, D, and E (see Fig. 7), predicted by the univariate and bivariate dimension-reduction methods, as well as results of a fourth-order Neumann expansion method and a Monte Carlo simulation (5000 samples).[23] The Neumann expansion solutions are obtained by following the development of Spanos and Ghanem.[32] As can be seen in Table 1, the Neumann expansion and dimension-reduction methods provide satisfactory results for prediction of standard deviations in comparison with simulation results. The accuracy of the response statistics from the bivariate dimension-reduction method is similar to the Neumann expansion method, and is slightly higher than the univariate dimension-reduction method. More importantly, however, a comparison of CPU times, shown in Fig. 8, indicates that the univariate dimension-reduction method is far more efficient than the Neumann expansion method. From Fig. 8, it can be seen that the bivariate dimension-reduction method also surpasses the computational efficiency of the fourth-order Neumann expansion method.

Table 1. Standard deviations of displacements and strains by various methods.[23]

Location	Response variable	Standard deviation of response			
		4th-order Neumann expansion method	Univariate dimension-reduction method	Bivariate dimension-reduction method	Monte Carlo simulation (5000 samples)
A	u_1	1.17×10^{-1}	1.15×10^{-1}	1.17×10^{-1}	1.19×10^{-1}
	ε_{11}	2.78×10^{-2}	2.72×10^{-2}	2.78×10^{-2}	2.79×10^{-2}
	ε_{22}	2.57×10^{-1}	2.51×10^{-1}	2.57×10^{-1}	2.58×10^{-1}
	ε_{12}	3.52×10^{-2}	3.45×10^{-2}	3.52×10^{-2}	3.54×10^{-2}
B	u_1	4.92×10^{-1}	4.83×10^{-1}	4.93×10^{-1}	4.95×10^{-1}
	ε_{22}	8.58×10^{-2}	8.41×10^{-2}	8.59×10^{-2}	8.49×10^{-2}
C	u_2	2.64×10^{-1}	2.58×10^{-1}	2.64×10^{-1}	2.66×10^{-1}
	ε_{11}	9.12×10^{-2}	8.92×10^{-2}	9.13×10^{-2}	9.28×10^{-2}
	ε_{22}	1.38×10^{-2}	1.35×10^{-2}	1.38×10^{-2}	1.41×10^{-2}
	ε_{12}	4.06×10^{-2}	3.97×10^{-2}	4.07×10^{-2}	4.13×10^{-2}
D	u_2	1.44	1.41	1.44	1.44
	ε_{22}	8.76×10^{-2}	8.53×10^{-2}	8.77×10^{-2}	8.52×10^{-2}
E	u_1	6.03×10^{-1}	5.91×10^{-1}	6.04×10^{-1}	5.98×10^{-1}
	u_2	1.46	1.44	1.47	1.46
	ε_{22}	8.74×10^{-2}	8.53×10^{-2}	8.76×10^{-2}	8.59×10^{-2}

Note: u_1 and u_2 are horizontal and vertical displacements, respectively; ε_{11} and ε_{22} represent normal tensorial strains; and ε_{12} represents tensorial shear strain.

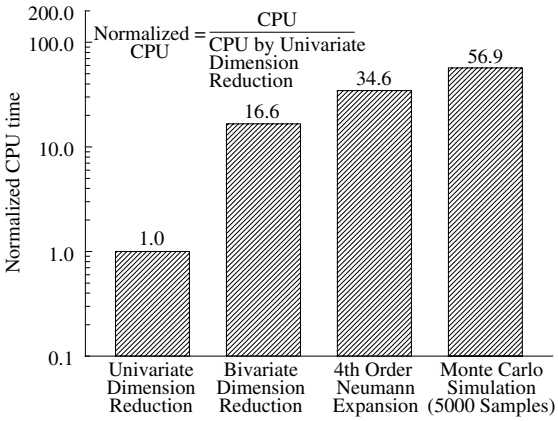

Fig. 8. Comparison of CPU times for moment analysis by various methods.[23]

6. Reliability Analysis

A fundamental problem in time-invariant reliability analysis entails calculation of a multi-fold integral[33–35]

$$P_F \equiv P(\boldsymbol{V} \in \Omega_F) = \int_{\Omega_f} f_V(\boldsymbol{v}) d\boldsymbol{v}, \tag{59}$$

where $\Omega_F \subset \Omega$ defines the failure domain and P_F is the probability of failure. For component reliability analysis, $\Omega_F = \{\boldsymbol{v} : y(\boldsymbol{v}) < 0\}$, where $y(\boldsymbol{v})$ represents a single performance function. For system reliability analyses involving r performance functions, $\Omega_F = \{\boldsymbol{v} : \bigcup_{k=1}^{r} y^{(k)}(\boldsymbol{v}) < 0\}$ and $\Omega_F = \{\boldsymbol{v} : \bigcap_{k=1}^{r} y^{(k)}(\boldsymbol{v}) < 0\}$ for series and parallel systems, respectively, where $y^{(k)}(\boldsymbol{v})$ represents the kth performance function. Nevertheless, for most practical problems, the exact evaluation of this integral, either analytically or numerically, is not possible since N is large and $y(\boldsymbol{v})$ or $y^{(k)}(\boldsymbol{v})$ are highly nonlinear functions of $\boldsymbol{v}$.

The most common approach to compute the failure probability in Eq. (59) involves the first- and second-order reliability methods (FORM/SORM),[33–35] which are based on linear (FORM) or quadratic approximation (SORM) of the limit-state surface at a most probable point (MPP). Experience has shown that FORM/SORM are sufficiently accurate for engineering purposes, provided that the limit-state surface at the MPP is close to being linear or quadratic, and no multiple MPPs exist.[35] Otherwise, the results of FORM/SORM should be interpreted with caution. Simulation methods involving sampling and estimation are well known in the statistics and reliability literature.[36–38] While simulation methods do not exhibit the limitations of approximate reliability methods, such as FORM/SORM, they generally require considerably more extensive calculations than the latter methods. Consequently, simulation methods are useful when alternative methods are inapplicable or inaccurate, and have been traditionally employed as a yardstick for evaluating approximate methods.

In this work, innovative response-surface approximations using multivariate function decomposition, which provides accurate and computationally efficient reliability estimates, are presented in the following subsection.

6.1. *Response surface generation*

Consider the univariate terms $y_i(v_i) \equiv y(c_1, \ldots, c_{i-1}, v_i, c_{i+1}, \ldots, c_N)$ in Eqs. (43) and (45). If for $v_i = v_i^{(j)}$, n function values

$$y_i(v_i^{(j)}) = y(c_1, \ldots, c_{i-1}, v_i^{(j)}, c_{i+1}, \ldots, c_N); \quad j = 1, 2, \ldots, n \tag{60}$$

are given, the function value for arbitrary v_i can be obtained using the Lagrange interpolation as

$$y_i(v_i) = \sum_{j=1}^{n} \phi_j(v_i) y_i\big(v_i^{(j)}\big), \tag{61}$$

where the Lagrange shape function $\phi_j(v_i)$ is defined as

$$\phi_j(v_i) = \frac{\prod_{k=1,k\neq j}^{n} \left(v_i - v_i^{(k)}\right)}{\prod_{k=1,k\neq j}^{n} \left(v_i^{(j)} - v_i^{(k)}\right)}. \tag{62}$$

Using Eq. (61), arbitrarily numerous function values of $y_i(v_i)$ can be generated if n function values are given. This is defined as the *univariate method*.[24]

The same concept can be applied to the bivariate terms $y_{i_1 i_2}(v_{i_1}, v_{i_2}) \equiv y(c_1, \ldots, c_{i_1-1}, v_{i_1}, c_{i_1+1}, \ldots, c_{i_2-1}, v_{i_2}, c_{i_2+1}, \ldots, c_N)$ in Eq. (45). If for $v_{i_1} = v_{i_1}^{(j_1)}$ and $v_{i_2} = v_{i_2}^{(j_2)}$, n^2 function values

$$y_{i_1 i_2}\big(v_{i_1}^{(j_1)}, v_{i_2}^{(j_2)}\big) \equiv y\big(c_1, \ldots, c_{i_1-1}, v_{i_1}^{(j_1)}, c_{i_1+1}, \ldots, c_{i_2-1}, v_{i_2}^{(j_2)}, c_{i_2+1}, \ldots, c_N\big); \quad j_1 = 1, 2, \ldots, n; \quad j_2 = 1, 2, \ldots, n \tag{63}$$

are given, the function value $y_{i_1 i_2}(v_{i_1}, v_{i_2})$ for arbitrary point (v_{i_1}, v_{i_2}) can be obtained using the Lagrange interpolation as

$$y_{i_1 i_2}(v_{i_1}, v_{i_2}) = \sum_{j_2=1}^{n} \sum_{j_1=1}^{n} \phi_{j_1}(v_{i_1}) \phi_{j_2}(v_{i_2}) y_{i_1 i_2}\big(v_{i_1}^{(j_1)}, v_{i_2}^{(j_2)}\big), \tag{64}$$

where shape functions $\phi_{j_1}(v_{i_1})$ and $\phi_{j_2}(v_{i_2})$ are already defined in Eq. (62). The resulting approximation is defined as the *bivariate method*.[24] Note that there are n and n^2 performance function evaluations (e.g. meshfree analyses) involved in Eqs. (61) and (64), respectively. Therefore, the total maximum cost for univariate method entails $nN + 1$ function evaluations, and for bivariate method, $N(N-1)n^2/2 + nN + 1$ maximum function evaluations are required. More accurate multivariate methods, such as an S-variate ($S > 2$) decomposition method, can be developed in a similar manner.

6.2. *Monte Carlo simulation*

For component reliability analysis, the Monte Carlo estimate of the failure probability employing S-variate response surface method is[24]

$$P_F \cong \frac{1}{N_S} \sum_{j=1}^{N_S} \mathbb{I}\Big[\hat{y}_S\big(\boldsymbol{v}^{(j)}\big) < 0\Big], \tag{65}$$

where $\boldsymbol{v}^{(j)}$ is the jth realization of $\boldsymbol{V}$, N_S is the sample size, and $\mathbb{I}[\cdot]$ is an indicator function such that $\mathbb{I} = 1$ if $\boldsymbol{v}^{(j)}$ is in the failure set (i.e. when $\hat{y}_S\big(\boldsymbol{v}^{(j)}\big) < 0$) and *zero* otherwise.

For system reliability analysis involving the union and intersection of r failure sets, similar response surface approximations can be developed for the kth performance function $y^{(k)}(\boldsymbol{v})$. Hence, the Monte Carlo estimate of the failure probability employing S-variate response surface method for series and parallel systems is

$$h_i \cong \begin{cases} \dfrac{1}{N_S} \displaystyle\sum_{j=1}^{N_S} \mathbb{I}\left[\bigcup_{k=1}^{r} \hat{y}_S^{(k)}\big(\boldsymbol{v}^{(j)}\big) < 0\right], & \text{series system} \\ \dfrac{1}{N_S} \displaystyle\sum_{j=1}^{N_S} \mathbb{I}\left[\bigcap_{k=1}^{r} \hat{y}_S^{(k)}\big(\boldsymbol{v}^{(j)}\big) < 0\right], & \text{parallel system} \end{cases}, \tag{66}$$

where $\mathbb{I}[\cdot]$ is another indicator function such that $\mathbb{I} = 1$ if $\boldsymbol{v}^{(j)}$ is in the system failure domain and *zero* otherwise. By setting $S = 1$ or 2, univariate or bivariate decomposition methods can be generated.

6.3. *Example 3: Reliability analysis of a plate with a hole*

Consider again the problem of a square plate with a hole under tension, as described in Example 2. In Example 3, the modulus of elasticity $E(\boldsymbol{x})$ is defined as a homogeneous, lognormal translation field $E(\boldsymbol{x}) = c_\alpha \exp[\alpha(\boldsymbol{x})]$, which has mean $\mu_E = 1$ unit and standard deviation $\sigma_E = 0.2$ or 0.5 unit. The image field $\alpha(\boldsymbol{x})$ is a *zero*-mean, homogeneous, Gaussian random field with standard deviation $\sigma_\alpha = \sqrt{\ln(1+\sigma_E^2/\mu_E^2)}$, $c_\alpha = \mu_E^2\sqrt{\mu_E^2+\sigma_E^2}$, and covariance function $\Gamma_\alpha(\boldsymbol{\xi}) = \sigma_\alpha^2 \exp[-|\boldsymbol{\xi}_1|/(bL) - |\boldsymbol{\xi}_2|/(bL)]$ with $b = 0.5$ unit. All other input parameters are the same as in Example 2.

The random field $\alpha(\boldsymbol{x})$ is parameterized using $N = 8$ in the K-L approximation. Hence, the input random vector $\boldsymbol{V} = \{V_1, \ldots, V_8\}^T$ becomes an eight-dimensional standard Gaussian random vector. The failure condition is defined when the von Mises equivalent stress $\sigma_A(V_1, \ldots, V_8)$ at point A exceeds the uniaxial yield strength S_y of the material.[24]

Figures 9(a) and 9(b) present failure probabilities for various yield strengths, predicted by the mean-point-based univariate and bivariate methods ($\boldsymbol{c} = \boldsymbol{0}$), as well as by the direct Monte Carlo simulation (10^5 samples). As can be seen in Fig. 9(a), when the uncertainty of elastic modulus is lower ($\sigma_E = 0.2$ unit), both univariate and bivariate methods provide satisfactory results in comparison with the simulation results. However, when a higher uncertainty is considered ($\sigma_E = 0.5$ unit), Fig. 9(b) indicates that the accuracy of the failure probability from the bivariate method is slightly higher than that from the univariate method. The number of function evaluations (i.e. meshfree analyses) for the proposed method with univariate and bivariate methods are only 33 and 481, respectively, when $n = 5$ and $N = 8$.

A comparison of total CPU times, shown in Fig. 10, indicates that both response decomposition methods are far more efficient than the Monte Carlo simulation. In calculating the CPU times, the overhead cost due to random field discretization, random number generation, and response surface approximations are all included. The overhead cost is comparable to the cost of conducting meshfree stress analysis in this particular problem. For this reason, the ratios of CPU times by bivariate and univariate methods and by Monte Carlo and univariate methods are respectively only 8 and 1080, as compared with 15 (= 481/33) and 3030 (= 1 000 000/33), when function evaluations alone are compared. For complex problems requiring more expensive response evaluations, the overhead cost is negligible. In that case, the CPU ratio should approach the ratio of function evaluations. Hence, the response decomposition methods are effective when a response evaluation entails costly meshfree or other numerical analysis.

The numerical results indicate that stochastic meshfree methods can generate accurate estimates of response moments and reliability. Although the same results can be produced using the well-established stochastic FEM, meshfree methods presented here do not require a structured mesh — a key advantage over FEM. It is generally recognized that successful meshing of complex geometric configurations

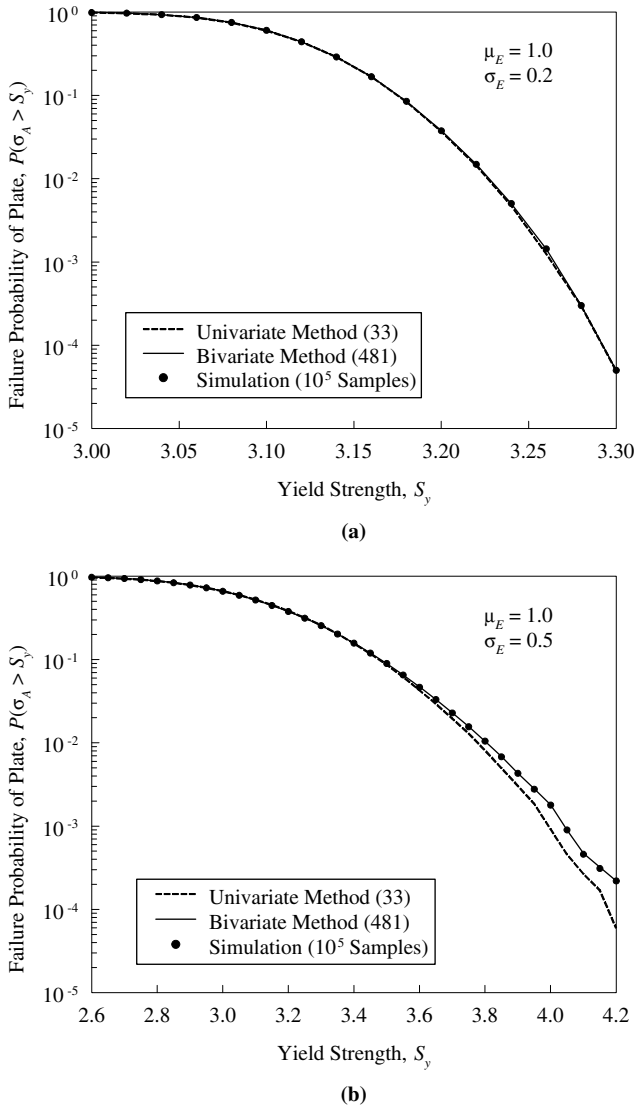

Fig. 9. Failure probability of square plate with a hole; (a) $\sigma_E = 0.2$; (b) $\sigma_E = 0.5$.[24]

can be difficult, time consuming, and expensive. This issue is further exacerbated when solving solid-mechanics problems characterized by a continuous change of the domain geometry, such as crack propagation in solids and metal forming, where a large number of automated remeshings are required due to moving cracks or mesh distortion. Stochastic meshfree methods are ideal candidates for solving these special classes of problems. Nevertheless, the computational cost of deterministic meshfree method is still much higher than that required by low-order FEM. Therefore, breakthrough research focused on enhancing speed and robustness of

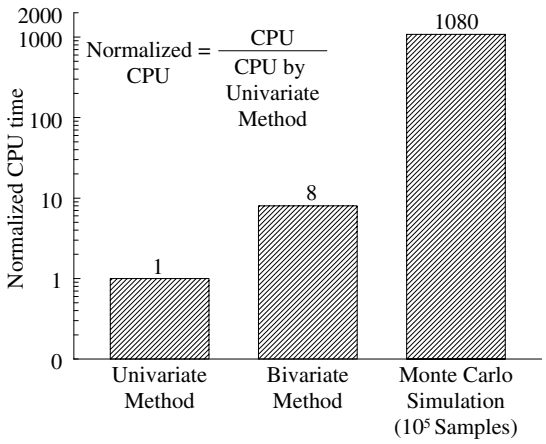

Fig. 10. Comparison of CPU times for reliability analysis by various methods.[24]

meshfree methods is required for their effective implementation into stochastic mechanics.

7. Conclusions and Outlook

This article has focused on meshfree methods for potential applications in stochastic mechanics and reliability. An exposition involving a brief summary of meshfree formulation, spectral representation of random field, multivariate function decomposition, statistical moment analysis, and reliability analysis has been presented. By avoiding burdensome meshing or remeshing required by the commonly-used finite element method, meshfree methods provide an attractive alternative to the finite element method for solving computational mechanics problems. For the same reason, the meshfree methods are effective in solving integral equations for spectral representation of a random field over a complex arbitrary domain. Numerical results indicate that stochastic meshfree methods, employed in conjunction with dimension-reduction and response-decomposition methods, yield accurate and computationally efficient estimates of statistical moments and reliability.

Although significant strides have been made, stochastic meshfree methods still require considerable improvement before they equal the prominence of the stochastic finite element method. Breakthrough research on enhancing speed and robustness of meshfree methods is essential for their successful implementation into stochastic mechanics.

Acknowledgments

This work was supported by the U.S. National Science Foundation under Grant Nos. CMS-9900196 and DMI-0355487.

References

1. J. J. Monaghan, *Comput. Phys. Commun.* **48**, 89 (1988).
2. P. W. Randles and L. D. Libersky, *Comput. Method. Appl. M.* **139**, 375 (1996).
3. B. Nayroles, G. Touzot and P. Villon, *Comput. Mech.* **10**, 307 (1992).
4. T. Belytschko, Y. Y. Lu and L. Gu, *Int. J. Numer. Meth. Eng.* **37**, 229 (1994).
5. C. A. M. Duarte and J. T. Oden, *Numer. Meth. Part. D. E.* **12**, 673 (1996).
6. J. M. Melenk and I. Babuska, *Comput. Method. Appl. M.* **139**, 280 (1996).
7. W. K. Liu, S. Jun and Y. F. Zhang, *Int. J. Numer. Meth. Fl.* **20**, 1081 (1995).
8. S. N. Atluri and T. Zhu, *Comput. Method. Appl. M.* **22**, 117 (1998).
9. P. Lancaster and K. Salkauskas, *Math. Comput.* **37**, 141 (1981).
10. T. Belytschko, Y. Y. Lu and L. Gu, *Eng. Fract. Mech.* **51**, 295 (1995).
11. M. Fleming, Y. A. Chu, B. Moran and T. Belytschko, *Int. J. Numer. Meth. Eng.* **40**, 1483 (1997).
12. B. N. Rao and S. Rahman, *Comput. Mech.* **26**, 398 (2000).
13. B. N. Rao and S. Rahman, *Eng. Fract. Mech.* **70**, 1 (2003).
14. B. N. Rao and S. Rahman, *Int. J. Numer. Meth. Eng.* **59**, 197 (2004).
15. B. N. Rao and S. Rahman, *Int. J. Pres. Ves. Pip.* **78**, 647 (2001).
16. S. Rahman and B. N. Rao, *Int. J. Numer. Meth. Eng.* **50**, 1969 (2001).
17. S. Rahman and B. N. Rao, *Int. J. Solids. Struct.* **38**, 9313 (2001).
18. S. Rahman and H. Xu, *Int. J. Comput. Meth. Eng. Sci. Mech.* **6**, 41 (2005).
19. B. N. Rao and S. Rahman, *Comput. Mech.* **28**, 351 (2002).
20. S. Rahman and B. N. Rao, *Comput. Mech.* **28**, 365 (2002).
21. B. N. Rao and S. Rahman, *Comput. Mech.* **32**, 199 (2003).
22. S. Rahman and H. Xu, *Probabilist. Eng. Mech.* **19**, 393 (2004).
23. H. Xu and S. Rahman, *Int. J. Numer. Meth. Eng.* **61**, 1992 (2004).
24. H. Xu and S. Rahman, *Probabilist. Eng. Mech.* **20**, 239 (2005).
25. J. S. Chen and H. P. Wang, *Comput. Method. Appl. M.* **187**, 441 (2000).
26. W. B. Davenport and W. L. Root, *An Introduction to the Theory of Random Signals and Noise*, McGraw-Hill, New York, NY (1958).
27. M. Grigoriu, *J. Eng. Mech. ASCE.* **110**, 610 (1984).
28. M. Grigoriu, *Applied Non-Gaussian Processes: Examples, Theory, Simulation, Linear Random Vibration, and MATLAB Solutions*, PTR Prentice Hall, Englewood Cliffs, NJ (1995).
29. M. Grigoriu, *J. Eng. Mech. ASCE.* **124**, 121 (1998).
30. M. Rosenblatt, *Ann. Math. Stat.* **23**, 470 (1952).
31. M. Abramowitz and I. A. Stegun, *Handbook of Mathematical Functions*, 9th Edition, Dover Publications, Inc., New York, NY (1972).
32. R. G. Ghanem and P. D. Spanos, *Stochastic Finite Elements: A Spectral Approach*, Springer-Verlag New York, NY (1991).
33. H. O. Madsen, S. Krenk and N. C. Lind, *Methods of Structural Safety*, Prentice-Hall, Inc., Englewood Cliffs, NJ (1986).
34. R. Rackwitz, *Struct. Saf.* **23**, 365 (2001).
35. O. Ditlevsen and H. O. Madsen, *Structural Reliability Methods*, John Wiley & Sons Ltd., Chichester, United Kingdom (1996).
36. R. Y. Rubinstein, *Simulation and the Monte Carlo Method*, John Wiley & Sons, New York (1981).
37. H. Niederreiter and J. Spanier, *Monte Carlo and Quasi-Monte Carlo Methods*, Springer-Verlag, Berlin, Germany (2000).
38. W. R. Gilks, S. Richardson and D. J. Spiegelhalter, *Markov Chain Monte Carlo in Practice*, Chapman-Hall, London, United Kingdom (1996).